Shell model description of the phonon dispersion in La_2CuO_4

1992 J. Phys.: Condens. Matter 4 4759

(http://iopscience.iop.org/0953-8984/4/20/003)

J. Phys.: Condens. Matter 4 (1992) 4759–4767. Printed in the UK

Shell model description of the phonon dispersion in La_2CuO_4

S Koval†, R Migoni† and H Bonadeo‡

† Instituto de Física Rosario (CONICET-UNR), Boulevard 27 de Febrero 210 Bis, 2000 Rosario, Argentina

‡ División Física del Sólido, Comisión Nacional de Energía Atómica, Avenida Libertador 8250, 1429 Buenos Aires, Argentina

Received 9 January 1992

Abstract. The phonon dispersion in La_2CuO_4, a base compound for high-T_c superconductors, is analysed in terms of a shell model. Shell charges and core–shell interactions are considered as anisotropic tensors. Short-range potentials of Born–Mayer type are taken to act between shells of different ions. An anisotropic screening of the Coulomb interaction is incorporated in order to describe the observed degeneracy of LO and TO modes polarized parallel to the CuO_2 planes. The phonon energies measured for wavevectors along the three principal symmetry directions are adjusted for the first time with a shell model and a good simulation is achieved with a relatively low number of parameters. Copper–oxygen and lanthanum–oxygen interactions turn out to be of comparable magnitude and much stronger than the oxygen–oxygen interaction. The soft mode that leads to the tetragonal–orthorhombic transition is found to be most sensitive to the La–O interaction. This suggests that anharmonicity in this interaction may be responsible for the lattice instability.

1. Introduction

Despite many experimental and theoretical results indicating the relevance of strong electron correlations in the physical properties of high-T_c superconductors [1] (HTS), there are in addition many indications that the lattice dynamics may also play an important role [2]. The fact that a value of T_c for $Ba_{1-x}K_xBiO_3$ [3] almost as high as for $La_{1-x}Sr_xCuO_4$ arises from electron–phonon interactions [4] suggests that this mechanism or some extension of it to non-linear dynamics [5–7] should not be discarded.

The lattice dynamics of HTS is also important for understanding the anharmonic mechanisms which lead to soft phonon behaviour related to structural phase transitions (for example in La_2CuO_4 [8, 9]). It may also be relevant for the observed anomalies in the phonon spectrum of La_2CuO_4 [10–12].

Several model calculations of the phonon spectrum of pure and doped La_2CuO_4 have been performed [13–15]. First-principles calculations have been also carried out [16, 17]. However, the experimental data away from the Brillouin zone centre have not been analysed in these works. This information has been recently obtained in a comprehensive way by inelastic neutron scattering [12].

0953-8984/92/204759 + 09 $04.50

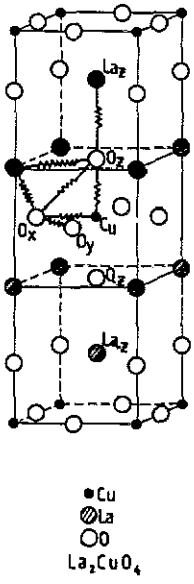

Figure 1. Conventional unit cell of body-centred tetragonal La_2CuO_4. For simplicity the La and O ions are shown as building basal planes; small displacements along the z axis are neglected. The springs join neighbouring ions which interact through Born–Mayer potentials.

The electronic polarizabilities of ions, in particular O^{2-}, play an important role in the lattice dynamics of ionic compounds. Moreover, it has been suggested that nonlinear polarizabilities may contribute to electron pairing in HTS [18]. Electron polarizabilities are explicitly taken into account in the shell model for lattice dynamics employed in [14, 15]. For these reasons, we shall use a shell model in the present work.

In the data obtained by Pintschovius *et al* [12], phonons with associated dipole moment parallel to the CuO_2 planes do not show the LO—TO splitting at the Γ point characteristic of ionic crystals. This is not the case for modes polarized along the c axis. This indicates the presence of an anisotropic screening of the ionic charges. Since this behaviour was not considered in the previous calculations [13–15], discrepancies are evident even at $k = 0$ when compared with the neutron diffraction data. We shall account for this effect by introducing an anisotropic screening in our model.

In the Raman spectrum [19], the lowest A_{1g} mode shows up about 2.4 THz higher than the corresponding mode as measured by Pintschovius *et al.* However, we choose to fit the Γ-point frequencies measured by neutron scattering, since they are compatible with the phonon energies for $k \neq 0$ in several directions of the Brillouin zone.

We shall analyse the room-temperature neutron scattering data [12], for which La_2CuO_4 is in its orthorhombic phase. The distortion with respect to the tetragonal structure is very small [20] and therefore we consider a pseudo-tetragonal structure with parameters $a = (a_0 + b_0)/8^{1/2} = 3.81$ Å and $c = 13.17$ Å, where a_0 and b_0 are the orthorhombic basal parameters. From [20] we take $z(O_z) = 0.182c$ for the position of the apex oxygen along the z axis with respect to the basal plane, and $z(La) = 0.362c$ for the analogous position of La. The crystal structure is schematically represented in figure 1.

2. The model

We consider a shell model where every ion κ is represented by a shell coupled to the core through a tensor $K_{\alpha\beta}(\kappa) = \delta_{\alpha\beta}K_\alpha(\kappa)$ with the symmetry of the corresponding ionic

site. The shell charges are represented by tensors $Y_{\alpha\beta}(\kappa)$ of the same symmetry while the total ionic charges are given, as usually, by isotropic tensors $Z_{\alpha\beta}(\kappa) = \delta_{\alpha\beta}Z(\kappa)$. Thus, for the oxygen O_z, we have $K_\perp(O_z) \equiv K_x(O_z) = K_y(O_z) \neq K_z(O_z) \equiv K_\parallel(O_z)$. In the case of the basal oxygen O_x we consider $K_y(O_x) = K_z(O_x)$ (although this is not imposed by symmetry) since this oxygen is fairly symmetrically surrounded by La in the plane perpendicular to x, whereas in the x direction it experiences effects from Cu ions. The same approximation is made for the shell charge of this ion. Obviously, for O_y we have $K_x(O_y) = K_y(O_x) \equiv K_\perp(O_{xy})$ and $K_y(O_y) = K_x(O_x) \equiv K_\parallel(O_{xy})$. However, as can be expected from the structure, we take $K_\parallel(O_z) \neq K_\parallel(O_{xy})$ and $K_\perp(O_z) \neq K_\perp(O_{xy})$.

The ion pairs Cu–O, La–O and O–O interact through a short-range Born–Mayer potential $V_{\kappa\kappa'} = a_{\kappa\kappa'}\, e^{-rb_{\kappa\kappa'}}$ between their shells, up to 4 Å. In addition there are Coulomb interactions between cores and shells of every ion. The macroscopic electric field associated with longitudinal polar phonons is anisotropically screened [21] by assuming a potential of the form

$$\varphi(r, \theta) = (e^2/r)\,\mathrm{Exp}\,(-\mathbb{K}(\theta)r) \tag{1}$$

where $\mathbb{K}(\theta) = \mathbb{K}_s \sin^2\theta$, θ being the angle between the z axis and the dipole moment of the longitudinal mode. This interaction is treated by Ewald's summation procedure as shown in the Appendix.

The initial parameter values were taken from [14]. The polarizability parameters were allowed to vary anisotropically during the fit of the experimental data. In this procedure, the root mean square (RMS) deviation for all measured phonon frequencies was considered and particular attention was paid to this deviation for the zone-centre phonons. The potential parameters $a_{\kappa\kappa'}$ and $b_{\kappa\kappa'}$ were adjusted by variation of the corresponding nearest-neighbour force constants $A_{\kappa\kappa'} = V''_{\kappa\kappa'}(r_{\kappa\kappa'})$ and $B_{\kappa\kappa'} = V'_{\kappa\kappa'}(r_{\kappa\kappa'})/r_{\kappa\kappa'}$. The parameter $\mathbb{K}_s$ for the inverse of the screening length was set equal to 0.5 $Å^{-1}$, which corresponds to a screening length of one half the basal lattice constant. This value leads to the observed degeneracy of the long-wave TO and LO phonons polarized perpendicularly to the c axis.

3. Results and discussion

During the fit of the experimental data, it was found that simulating anisotropy of the core–shell interaction and shell charge at Cu does not significantly improve the agreement. Therefore these tensors are considered isotropic. Moreover, for the same reason, all oxygen ionic charges are taken as equal. On the other hand, the fit procedure leads to significant anisotropy for both tensors $K_{\alpha\beta}$ and $Y_{\alpha\beta}$ of the O ions and the core–shell coupling $K_{\alpha\beta}$ of La. This was not the case for the La shell charge, and therefore it was taken as isotropic (see table 1).

A relatively large difference is also found between the shell charge and core–shell coupling tensors of the apex oxygen O_z and the corresponding quantities of the in-plane oxygens O_{xy}. Compare, for example, $K_\parallel(O_z)$ and $K_\perp(O_z)$ with $K_\parallel(O_{xy})$ and $K_\perp(O_{xy})$, respectively.

The potential parameters obtained from the fit are also given in table 1. It is, however, more meaningful to analyse the near-neighbour force constants A and B, given in table 2. These interactions are visualized by means of springs in figure 1. The values of these parameters follow a similar trend to those found in previous shell model calculations

Table 1. Shell model parameters derived from the fit to the data shown in figure 2. v_a is the primitive unit cell volume.

	Potential parameters	
Pairs	a (eV)	b (Å^{-1})
Cu–O	437.93	2.45
O–O	399.82	3.27
La–O	18967.35	3.87

Charges (e)		Core–shell couplings (e^2/v_a)	
Z(Cu)	2.00	K(Cu)	3007.20
Z(O)	−1.94	$K_\parallel(O_{xy})$	360.75
Z(La)	2.84	$K_\perp(O_{xy})$	110.87
Y(Cu)	2.00	$K_\parallel(O_z)$	115.38
$Y_\parallel(O_{xy})$	−3.43	$K_\perp(O_z)$	35.24
$Y_\perp(O_{xy})$	−2.03	$K_\parallel$(La)	105.83
$Y_\parallel(O_z)$	−1.30	$K_\perp$(La)	550.95
$Y_\perp(O_z)$	−2.20		
Y(La)	3.19		

Table 2. Force constants for the neighbouring ions joined by springs in figure 1 and corresponding distances r.

Pairs	$A(e^2/v_a)$	$B(e^2/v_a)$	r (Å)
Cu–O_{xy}	163.80	−35.08	1.905
Cu–O_z	49.05	−8.35	2.397
O_x–O_y	4.27	−0.49	2.694
O_z–O_{xy}	1.28	−0.13	3.062
La_z–O_z	195.88	−21.36	2.371
La–O_{xy}	71.00	−6.97	2.633
La_{-z}–O_z	44.15	−4.14	2.756

[14–15]. The Cu–O and La–O forces are the largest and comparable in magnitude while the O–O interaction is about two orders of magnitude smaller.

The calculated dispersion curves are compared with the experimental data in figure 2. We arrive at these results by using a total of 22 independent model parameters: 6 for the interionic potentials, 13 polarizability parameters and 3 ionic charges. This is a relatively satisfactory number of parameters when compared with the 34 variables needed to obtain a fit of similar quality with a rigid-ion model for the dispersion curves of La_2NiO_4 [21]. The same model applied to La_2CuO_4 involves even more difficulties, as has been mentioned [12]. The advantages of our shell model in this respect are therefore evident.

We attempted to simulate the anisotropic screening of the macroscopic electric field by introducing large polarizability components parallel to the basal planes, but this procedure did not lead to the observed degeneracy of the E_u modes without spoiling the whole spectrum. On the other hand, with the potential of equation (1) we observe in figure 2 that the branches of transverse modes Δ_3 and Σ_3 become degenerate at $\boldsymbol{k} = 0$ with longitudinal modes corresponding to Δ_1 and Σ_1 branches respectively (compare E_u

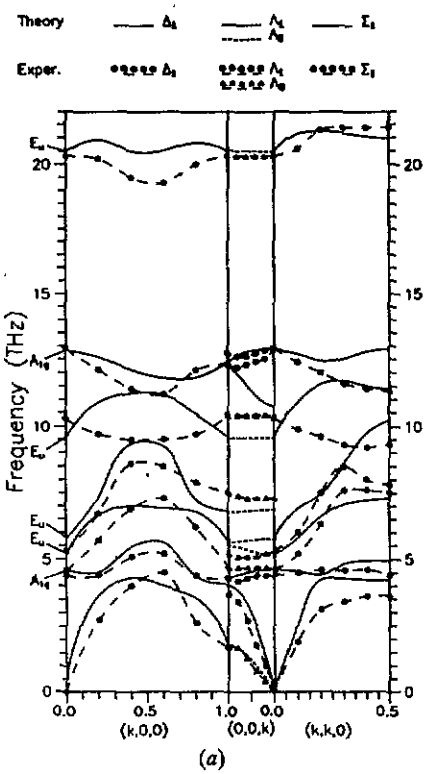

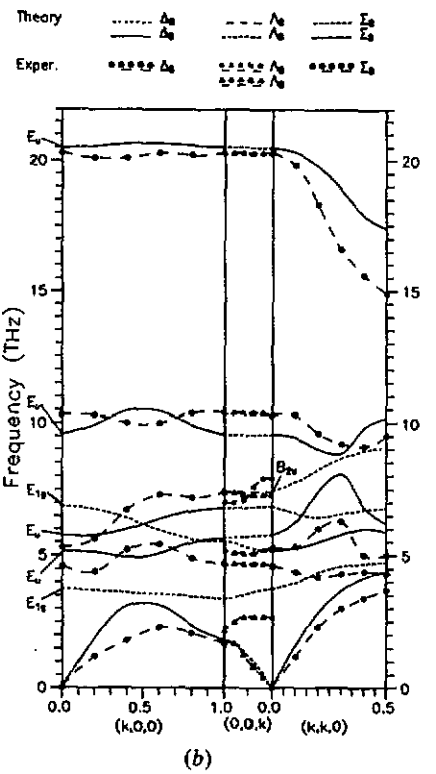

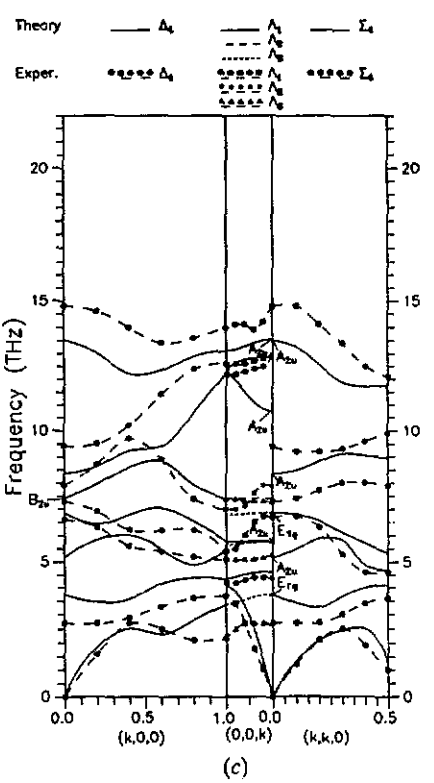

Figure 2. Theoretical and experimental phonon dispersion curves in the main symmetry directions of La_2CuO_4. The wavevector k is in units of $(2\pi/a, 2\pi/a, 2\pi/c)$. The dashed lines through the experimental points are guides to the eye. The modes in directions $(k, 0, 0)$ and $(k, k, 0)$ are separated as follows: (a) longitudinal modes, (b) transverse modes $\perp z$ and (c) transverse modes $\| z$. For the direction $(0, 0, k)$ in each case are shown those branches which are compatible with those in the other directions.

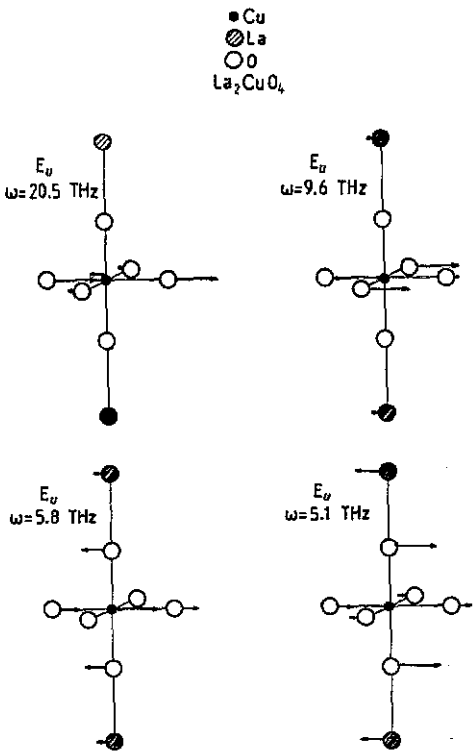

Figure 3. Eigenvectors of the optical E_u modes. All of them present an LO–TO degeneracy.

modes in figures 2(*a*) and 2(*b*)). On the other hand, *z*-polarized modes A_{2u} are not screened (see figure 2(*c*)) and in particular the second highest one shows a significant LO–TO splitting.

The overall description of the dispersion curves is quite satisfactory. Most of the experimental branches are quantitatively reproduced, and even when this is not so, a qualitative agreement is observed with only few exceptions. The overall RMS frequency difference is $\Delta = \langle(\Delta\nu)^2\rangle^{1/2} = 0.8$ THz. Satisfactory agreement is also obtained for the Γ modes, with $\Delta(\Gamma) = 0.6$ THz.

The highest LO modes (symmetries Δ_1 and Σ_1) at (0.5, 0, 0) and (0.5, 0.5, 0) are breathing-type motions of the in-plane oxygens around the Cu ions. Note that the zone boundary in the (k, 0, 0) direction is located about $k = 0.5$. The small softening of the corresponding branch Δ_1 when approaching (0.5, 0, 0) is qualitatively reproduced by the model without introduction of a breathing degree of freedom for the Cu shell. On the other hand, the highest Σ_1 branch grows to higher frequencies when approaching (0.5, 0.5, 0). It should be mentioned that the behaviour of these branches appears to be related to the observation of additional neutron groups between 14 and 15 THz, which obviously cannot be explained within the framework of a harmonic model.

By analysis of the eigenvectors of the Γ modes, we found them to be similar to those in [15] except for the ones depicted in figure 3, all of which are E_u modes. These modes are precisely the ones which are affected by the anisotropic screening, a mechanism not included in the previous calculation [15].

We have analysed the stability of the lattice modes with respect to variations of the model parameters. A softening of the TA(Σ_4) branch with temperature is experimentally

Table 3. Relative parameter variations which render unstable the tilting mode related to the tetragonal–orthorhombic transition.

B(La–O)	B(Cu–O)	A(La–O)	A(Cu–O)	$K_\perp(O_z)$
+0.0067	−0.0212	+0.0214	−0.0977	−0.3036

observed near the zone boundary, and the instability of the zone boundary mode ω_{sm} corresponds to the tetragonal–orthorhombic transition [8, 9]. This TA branch is well reproduced in our calculation and in table 3 we give the interaction parameters which most significantly affect ω_{sm}. We give for each parameter the relative variation which leads to $\omega_{sm} = 0$. It can be seen that the most relevant influence arises from the transverse La–O interaction. Since all La–O pairs interact through the same potential, all force constants B(La–O) are simultaneously varied at the same rate. Note that ω_{sm} is much less sensitive with respect to variations of the core–shell coupling $K_\perp(O_z)$. The renormalization of the core–shell interaction at oxygen due to a local anharmonic electron–ion interaction has been considered in a one-dimensional model to be responsible for the tetragonal–orthorhombic structural instability [22]. Our results suggest that an anharmonic shell–shell interaction between La and O is more likely to be responsible for this instability. This situation appears to be the inverse of the one found in oxide ABO_3 perovskites where the ferroelectric soft mode is more sensitive to variations of the oxygen core–shell interaction than to the transition metal–oxygen (B–O) interaction [23]. In agreement with the situation we encounter in La_2CuO_4, the softening of the tilting mode has been described on the basis of weak anharmonic perturbation theory for interactions between the various ion pairs [24]. The anharmonic force constants were determined from several anharmonic properties and the La–O force constant turned out to be the strongest.

We found that additional modes easily become unstable with relatively small variations of some parameters, although not so small as the values shown in table 3 for the case of the tilting mode. One of them is a Σ_3 mode towards the zone boundary, which corresponds to an in-plane rotation of O_{xy} ions around Cu. This is mostly affected by B(La–O). Another two such modes are the lowest E_u mode at $k = 0$, with displacement pattern shown in figure 3, and the longitudinal acoustic mode of Δ_1 symmetry towards the zone boundary, with similar ionic displacements. Both are greatly affected by variations of A(Cu–O). The rotational mode and the lowest E_u mode were also found to be unstable in a non-empirical calculation with a potential-induced breathing model [16].

4. Conclusion

We have simulated well the phonon dispersion in La_2CuO_4 using a shell model with a reasonable number of parameters. The inclusion of anisotropic polarizability parameters allows us to improve the fit to experimental data. The LO–TO degeneracy of Γ modes polarized parallel to the CuO_2 basal planes is achieved by considering an anisotropically screened Coulomb potential. The high-frequency breathing modes are satisfactorily described without introduction of any *ad hoc* mechanism. The softening of the tilting

mode responsible for the tetragonal–orthorhombic transition seems to be governed by La–O interactions.

Acknowledgments

We acknowledge support from the Consejo Nacional de Investigaciones Científicas y Técnicas.

Appendix

The Fourier transform of the screened Coulomb potential in equation (1) may be written as

$$\varphi(Q,\theta) = 4\pi e^2/(Q^2 + \mathbb{K}^2(\theta))\ \varphi(Q,\theta) = (4\pi e^2/Q^2)[1 - \mathbb{K}^2(\theta)/(Q^2 + \mathbb{K}^2(\theta))]. \tag{A1}$$

This separation into two terms of the Fourier transform may be reflected in the following real-space expression:

$$\varphi(r,\theta) = e^2/r + \varphi_s(r,\theta). \tag{A2}$$

Ewald's procedure applied to obtain the Coulomb coefficients for this potential consists of writing the expression as the sum of the following two contributions,

$$\varphi(r,\theta) = \varphi^{(1)}(r) + \varphi^{(2)}(r,\theta) = [e^2/r - \varphi^{G}(r)] + [\varphi^{G}(r) + \varphi_s(r,\theta)] \tag{A3}$$

where $\varphi^{G}(r)$ is the potential due to a Gaussian distribution with total charge e. The contribution to the Coulomb coefficients arising from the first term is conveniently expressed as a sum over the direct lattice and has the usual form for unscreened potential [25]. The analogous contribution of the second term converges more rapidly as the following sum over the reciprocal lattice:

$$\varphi^{(2)}_{\alpha\beta}(\kappa\kappa'|\boldsymbol{k},\theta) = \frac{1}{v_a}\sum_{\boldsymbol{G}} (\boldsymbol{G}+\boldsymbol{k})_\alpha(\boldsymbol{G}+\boldsymbol{k})_\beta \varphi^{(2)}(\kappa\kappa'|\|\boldsymbol{G}+\boldsymbol{k}\|,\theta)\ \mathrm{Exp}\,[-\mathrm{i}\boldsymbol{G}\cdot(\boldsymbol{r}_{\kappa'} - \boldsymbol{r}_\kappa)] \tag{A4}$$

where

$$\varphi^{(2)}(\kappa\kappa'|Q,\theta) = (4\pi e^2/Q^2)[\mathrm{Exp}\,(-Q^2/4\rho_0^2) - \mathbb{K}^2(\theta)/(Q^2 + \mathbb{K}^2(\theta))] \tag{A5}$$

where ρ_0^{-1} is the spread of the Gaussian charge distribution, which is conveniently chosen for convergence. The angle θ in the above coefficients is defined as that between $\boldsymbol{k}$ and the z direction. This defines the orientation of the dipole moment with respect to the z axis for longitudinal polar modes, which are the only ones with an associated macroscopic field to be screened. For other modes, θ has no precise relation to their polarizations, but they do not give rise to a macroscopic field.

References

[1] For reviews see
Lynn J W (ed) 1990 *High Temperature Superconductivity* (Berlin: Springer)
Woods Halley J. (ed) 1988 *Theories of High Temperature Superconductivity* (Reading, Massachusetts: Addison-Wesley)

[2] Barišič S 1991 *Int. J. Mod. Phys.* B **5** 2439
[3] Mattheiss L F, Gyorgy E M and Johnson D W Jr 1988 *Phys. Rev.* B **37** 3745
Cava R J, Batlogg B, Krajewski J J, Farrow R, Rupp L W Jr, White A E, Short K, Peck W F and Kometani T 1988 *Nature* **332** 814
[4] Shirai M, Suzuki N and Motizuki K 1990 *J. Phys.: Condens. Matter* **2** 3553
Liechtenstein A I, Mazin I I, Rodriguez C O, Jepsen O, Andersen O K and Methfessel M 1991 *Phys. Rev.* B **44** 5388
[5] Hardy J R and Flocken J W 1988 *Phys. Rev. Lett.* **60** 2191
[6] Plakida N M 1989 *Phys. Scr.* **T29** 77
[7] Frick M, von der Linden W, Morgenstern I and de Raedt H 1990 *Z. Phys.* B **81** 327
[8] Birgeneau R J, Chen C Y, Gabbe D R, Jenssen H P, Kastner M A, Peters C J, Picone P J, Thio Tineke, Thurston T R, Tuller H L, Axe J D, Böni P and Shirane G 1987 *Phys. Rev. Lett.* **59** 1329
[9] Böni P, Axe J D, Shirane G, Birgeneau R J, Gabbe D R, Jenssen H P, Kastner M A, Peters C J, Picone P J and Thurston T R 1988 *Phys. Rev.* B **38** 185
[10] Rietschel H, Pintschovius L and Reichardt W 1989 *Physica* C **162–164** 1705
[11] Pintschovius L 1990 *Proc. Third Int. Conf. on Phonon Physics* ed S Hunklinger, W Ludwig and G Weiss (Singapore: World Scientific) p 217
[12] Pintschovius L, Pyka N, Reichardt W, Rumiantsev A Yu, Ivanov A and Mitrofanov N 1990 *Proc. Int. Seminar on High Temperature Superconductors* ed V L Aksenov, N N Bogolubov and N M Plakida (Singapore: World Scientific) p 36
[13] For a review, see
Feile R 1989 *Physica* C **159** 1
[14] Prade J, Kulkarni A D, de Wette F W, Kress W, Cardona M, Reiger R and Schröder U 1987 *Solid State Commun.* **64** 1267
[15] Monstoller M, Zhang J, Rao A M and Eklund P C 1990 *Phys. Rev.* B **41** 6488
[16] Cohen R E, Pickett W E, Krakauer H and Boyer L L 1988 *Physica* B **150** 61
[17] Cohen R E, Pickett W E and Krakauer H 1989 *Phys. Rev. Lett.* **62** 831
[18] Bussmann-Holder A, Simon A and Büttner H 1989 *Phys. Rev.* B **39** 207
Bussmann-Holder A, Bishop A R and Batistić I 1991 *Phys. Rev.* B **43** 13728
[19] See [15] and references therein
[20] Longo J M and Raccah P M 1973 *J. Solid State Chem.* **6** 526
[21] Pintschovius L, Bassat J M, Odier P, Gervais F, Chevrier G, Reichardt W and Gompf F 1989 *Phys. Rev.* B **40** 2229
[22] Bussmann-Holder A, Migliori A, Fisk Z, Sarrao J L, Leisure R G and Cheong S W 1991 *Phys. Rev. Lett.* **67** 512
[23] Migoni R, Bilz H and Bäuerle D 1976 *Phys. Rev. Lett.* **37** 1155
[24] Heid R and Rietschel H 1991 *Phys. Rev.* B **44** 734
[25] Maradudin A A, Montroll E W, Weiss G H and Ipatova I P 1971 *Theory of Lattice Dynamics in the Harmonic Approximation, Solid State Physics* Suppl 3 ed 2 (London: Academic) ch 6